Finite element analysis of the lumbar spine with a new cage using a topology optimization method

Article *in* Medical Engineering & Physics · February 2006

DOI: 10.1016/j.medengphy.2005.03.007 · Source: PubMed

6 authors, including:

Zheng-Cheng Zhong

22 PUBLICATIONS **875** CITATIONS

SEE PROFILE

Shun-Hwa Wei

National Yang Ming University

57 PUBLICATIONS **1,341** CITATIONS

SEE PROFILE

Chi-Kuang Feng

Taipei Veterans General Hospital

20 PUBLICATIONS **532** CITATIONS

SEE PROFILE

Chen-Sheng Chen

National Yang Ming University

64 PUBLICATIONS **2,564** CITATIONS

SEE PROFILE

Available online at www.sciencedirect.com
SCIENCE DIRECT
Medical Engineering & Physics 28 (2006) 90–98
Medical Engineering & Physics
www.elsevier.com/locate/medengphy

Technical note

Finite element analysis of the lumbar spine with a new cage using a topology optimization method

Zheng-Cheng Zhong [a], Shun-Hwa Wei [a], Jung-Pin Wang [b], Chi-Kuang Feng [c], Chen-Sheng Chen [a,*], Chung-huang Yu [a]

[a] *Institute of Rehabilitation Science and Technology, National Yang-Ming University, 155 Li-Nung St., Sec. 2, Taipei, Taiwan*
[b] *Department of Orthopaedic Surgery, Mackay Memorial Hospital, Taipei, Taiwan*
[c] *Department of Orthopaedic Surgery, Veteran General Hospital-Taipei, Taipei, Taiwan*

Received 24 January 2005; received in revised form 24 January 2005; accepted 4 March 2005

Abstract

In recent years, degenerative spinal instability has been effectively treated with a cage. However, little attention is focused on the design concept of the cage. The purpose of this study was to develop a new cage and evaluate its biomechanical function using a finite element method (FEM).

This study employed topology optimization to design a new cage and analyze stress distribution of the lumbar spine from L1 to L3 with a new cage by using the commercial software ANSYS 6.0. A total of three finite element models, namely the intact lumbar spine, the spine with double RF cages, and with double new cages, were established. The loading conditions were that 10 N m flexion, extension, lateral bending, and torsion, respectively, were imposed on the superior surface of the L1 vertebral body. The bottom of the L3 vertebral body was constrained completely.

The FEM estimated that the new cage not only could be reduced to 36% of the volume of the present RF cage but was also similar in biomechanical performance such as range of motion, stress of adjacent disc, and lower subsidence to the RF cage. The advantage of the new cage was that the increased space allowed more bone graft to be placed and the cage saved material. The disadvantage was that stress of the new cage was greater than that of the RF cage.

Keywords: Cage; Finite element method; Biomechanics

1. Introduction

Posterior lumbar interbody fusion is an effective technique for treating degenerative spinal instability, and the final goal of the procedure is to restore disc height, enlarge the stenotic foramen, and support the anterior spinal column. The procedure often obtains the bone grafts from the iliac crests. However, this is associated with donor site morbidity, postoperative discomfort, and infection. Therefore, Bagby [1] developed the lumbar interbody fusion cage during the 1980s.

The spinal interbody fusion cage is a small, porous, hollow implant, either cylindrical or nearly cuboid in shape. It can replace the degenerative disc and distract the intervertebral body, thus restoring physiological disc height. The bone grafts can be inserted into the hollow and porous cage allowing the growth of bone through the cage, resulting in bony fusion. Furthermore, it can increase the mechanical strength and fusion rate.

Since 1994, more than 80,000 lumbar interbody fusion cages have been implanted for the treatment of degenerative discs [2], and the excellent fusion rates have been reported in some clinical experimental data [3–6]. Although the initial clinical reports were positive and the cage is used more widely, severe complications and poor outcomes such

* Corresponding author. Tel.: +886 2 28216149; fax: +886 2 28270140.
E-mail address: cschen@ym.edu.tw (C.-S. Chen).

1350-4533/$ – see front matter © 2005 IPEM. Published by Elsevier Ltd. All rights reserved.
doi:10.1016/j.medengphy.2005.03.007

as subsidence, dislodgement, or adjacent disc degeneration can happen when using implants [2,7–9].

Currently, many kinds of spinal cage designs are available (BAK, Sulzer-Spinetech, Minneapolis, Minn. Ray Cage, Surgical Dynamics, Norwalk Conn.; Brantigan I/F, Depuy-Acromed Corp., Cleveland, OH; Contact Fusion Cage, Stratec, Oberdorf, Switzerland; Harms mesh cage, Depuy-Acromed Corp., Cleveland, OH; SynCage, Mathys Medical Ltd., Bettlach, Switzerland; and others) and widely utilized, but little scientific or technical literature has reported on their design concepts.

The finite element model (FEM) has the advantage of easily modifying cage geometry without the need for cadaveric or animal specimens. Therefore, the finite element method has been used widely for analyzing biomechanical problems and has been successfully used in many other studies on the lumbar spine [10–16]. On the other hand, topological optimization is a form of shape optimization aimed at finding the best use of material for a body. The best use of material, in the case of topological optimization, represents the "maximum-stiffness" design. Consequently, the study took advantage of the topological optimization in the finite element analysis to design a new cage and evaluate its biomechanical behavior.

The main clinical parameters that were considered were the range of motion (ROM), the maximum subsidence of the cage, the maximum dislodgement of the cage, and the stress on the adjacent disc.

2. Materials and methods

A total of three FEMs of the lumbar spine were constructed in this study. The first one was the intact lumbar spine. The other two fusion models were the lumbar spine implanted with a contemporary cage and with a new cage.

2.1. FEM of the intact lumbar spine

To create this model, computed tomography (CT) scans of the lumbar spine from L1 to L3 of a 19-year-old healthy young male were obtained. The commercially available finite element program ANSYS 6.0 (Swanson Analysis System Inc., Houston, TX) was applied to model the spinal segments. The FEM of the ligamentous lumbar spine included vertebrae, intervertebral discs, endplates, posterior elements, and a number of ligaments: supraspinous, interspinous, ligamentum flavum, transverse, posterior longitudinal, anterior longitudinal, and capsular.

The material properties were assumed to be homogeneous and isotropic, and the data were adopted from the literature [17–19] and are given in Table 1. Ligaments were simulated by two-node link elements with resistance tension only, and elements were arranged in the anatomical direction given by the literature [20]. The cross-sectional area of each ligament was obtained from the literature [17] and are listed in Table 1. A 20-node solid element was used for modeling the cortical bone, cancellous bone, endplate, and disc and is listed in Table 2. The discal annulus consists of fibers embedded in the ground substance. Annulus fibers were modeled by the two-node link elements with resistance tension only and placed at an angle of 30°. The facet joint was treated as a nonlinear three-dimensional contact problem using surface-to-surface contact elements, and the friction coefficient was set at 0.1 [15]. The initial distance between adjacent facet surfaces was 1 mm. The FEM of the intact lumbar spine (INT) consisted of 2460 elements and 9602 nodes (Fig. 1). This INT model was validated in previous studies [21–23], in which the stiffness of

Table 1
Material properties used in FEM of the lumbar spine [17–19]

Material	Young's modulus (E, MPa)	Poisson ratio	Cross-section area (mm^2)
Cortical bone	12000	0.3	–
Cancellous bone	100	0.2	–
Posterior elements	3500	0.25	–
Disc			
Nucleus	1	0.499	–
Ground substance	4.2	0.45	–
Fiber	450	–	0.76
Endplate	24	0.4	
Ligament			
ALL	20	–	63.7
PLL	20	–	20
TL	58.7	–	3.6
LF	19.5	–	40
ISL	11.6	–	40
SSL	15	–	30
CL	32.9	–	60
Spinal instrumentation (titanium alloy)	110000	0.28	
Spinal cage (titanium alloy)	110000	0.28	–

ALL, anterior longitudinal ligament; PLL, posterior longitudinal ligament; TL, transverse ligament; LF, ligamentum flavum; ISL, interspinous ligament; SSL, supraspinous ligament; CL, capsular ligament.

Table 2
Element type used in the FEM of the lumbar spine

Intervertebral body		Element type
Vertebrae	Cortical bone, Cancellous bone	20-Node Solid 95
Posterior element		20-Node Solid 95
Disc	Ground substance	20-Node Solid 95
	Nucleus	20-Node Solid 95
	Fiber	2-Node Link 10
Spinal cage	Cage	20-Node Solid 95
	Contact surface	8-Node Contact 174
	Target surface	Target 170
Facet joint	Contact surface	8-Node Contact 174
	Target surface	Target 170
Ligament	ALL, PLL, TL, LF, ISL, SSL, CL	2-Node Link 10
Spinal instrumentation	Rod and screw	2-Node Beam 188

this INT model was compared to the stiffness of the cadaveric specimen in the in vitro test.

2.2. FEM of lumbar interbody fusion

To simulate the posterior lumbar interbody fusion, the laminectomy and partial discectomy were performed on the L2–L3 motion segments. The posterior elements, supraspinous, interspinous, ligamentum flavum ligaments, and the partial disc, were removed and replaced by the implanted spinal cage and instrumentation system.

In this model, two pedicle screws ($r = 6$ mm) were simulated to be inserted through the pedicle and connected by two rods ($r = 6$ mm) modeled with three-dimensional beam elements. Two RF (A-Spine Inc., Japan) cages (12 mm × 16 mm × 24 mm) were placed between the vertebral bodies within the two-thirds of the disc space in the transverse plane. The bone–cage interface was modeled by surface-to-surface contact elements to simulate the early postoperative stage after implantation of the spinal cage. These contact elements are able to transmit compression forces but not tension. Most cages have small teeth on the contact surfaces that are supposed to prevent movement of the cage, so a higher friction coefficient of 0.8 was defined between the cage and the adjacent vertebrae [15]. For the fusion model, two types of models were built by changing the parameters for examination of the effects of the RF cages compared with a new design cage. This FEM of the lumbar spine with two RF cages (LS-RF) (12 mm × 16 mm × 24 mm) consisted of 16,808 elements and 26,529 nodes (Fig. 2).

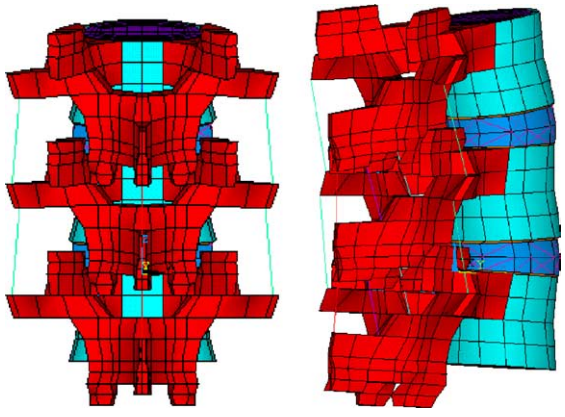

Fig. 1. The FEM of intact lumbar spine L1–L3.

2.3. Topology optimization

In the clinic, the spinal surgery was performed under consideration of the spinal instability, so the spinal fusion aimed to restore spinal stability using a cage to replace the degenerated disc. Consequently, this study focuses on maximizing the global structural stiffness by maximizing the clinical stability. However, the spinal cage is only a simple support and its main purpose is to assist in fusing the bone graft into the vertebral body. If a cage is able to increase its inner space so as to make it possible to place more bone graft while not losing too much spinal stiffness, this kind of new cage is more appropriate for clinical fusion procedures because it stimulates bony fusion while avoiding subsidence [24]. For this purpose, this study employed topology optimization to seek the cage region transmitting small loads with a view to removing this unnecessary material in favour of placing bone graft. This study applied the topological optimization in the ANSYS 6.0 software to design a new cage. Our design concepts aimed to reduce the volume of the spinal cage so as to increase the space for bone graft ingrowth. However, this new design needed to stabilize motion of the segment under a volume reduction of the cage. The theory of topological optimization seeks to minimize the energy of structural compliance, which is the so-called objective function. Minimizing the compliance is equivalent to maximizing the global structural stiffness [25], so the standard formulation of topological optimization defined the problem as minimizing the structural compliance while satisfying a constraint on the volume (V) of the structure. The optimization problem is as follows:

$$\text{objective function}: \text{minimize}\,(U_c) \tag{1}$$

$$\text{limitation}: 0 < \eta_i < 1 \quad (i = 1, 2, 3, \ldots, n) \tag{2}$$

$$V \le V_o - V^* \tag{3}$$

$$V = \sum_i \eta_i V_i \tag{4}$$

$$E_i = E(\eta_i) \tag{5}$$

$$\{\sigma_i\} = [E_i]\{\varepsilon_i\} \tag{6}$$

where U_c is the energy of structural compliance, η_i the internal pseudodensities that are assigned to each finite element (i) in the topology problem, V the computed volume, V_o the original volume, V^* the amount of material to be removed,

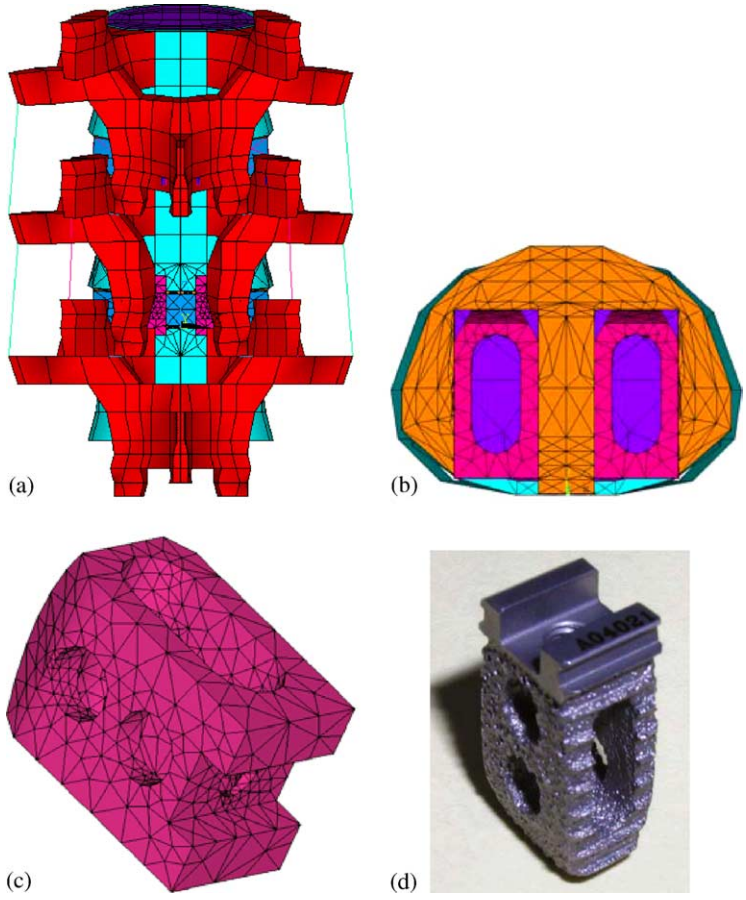

Fig. 2. (a) The LS-RF model consisted of fusion spine with the two RF cages and laminectomy for decompression, (b) the location of the RF cages in the LS-RF model, (c) FEM of the RF cage, and (d) the product of RF cage.

V_i the volume of element i, E_i the elasticity tensor for each element, E the elasticity tensor, σ_i the stress vector of element i, and ε_i is the strain vector of element i.

The density variable, η, was varied between 0 and 1, where η_i close to 0 represents material to be removed; η_i close to 1 represents material that should be retained. The topological optimization of the structural simulation was performed in flexion since the lumbar spine has greater ROM during daily activity. The program was expected to reduce the volume by 50% and iterate 20 times. The convergence tolerance was defined as 0.0001. From the iterations of the optimization, we could find a reasonable distribution of the material in a new cage.

2.4. Boundary and loading condition

In these models, the inferior surfaces of the L3 vertebral body were constrained completely. The loading condition in FEM refers to Yamamoto et al.'s in vitro study and is justified from their study [26]. The lumbar spine was subjected to the maximum possible load without causing spinal injury, so the 10 N m flexion, extension, torsion, and lateral bending moment, respectively, with the 150 N of the preload were imposed on the superior surfaces of the L1 vertebral body.

3. Results

This study presents the results in two parts. First, the new design cage modified from the RF cage is presented. Second, the biomechanical behavior of the lumbar spine with the RF and the new cage, respectively, are compared to that of the intact lumbar spine.

3.1. Topology analysis

The final design of this new cage was obtained from the topology optimization. Most loads were transferred to the anterior of the cage as shown in Fig. 3, so the study modified the RF cage accordingly to form a new cage. The volume of the new design was reduced from 2058 mm^3 to 1603 mm^3. The FEM, consisting of the new cage and lumbar spine with laminectomy (LS-NEW), was reconstructed. The LS-NEW model consisted of 22,024 elements and 44,004 nodes.

3.2. Biomechanical analysis of the three FEMs

3.2.1. Range of motion

This study indicated that these two fusion models were able to achieve spinal stability, in which the ROM of the

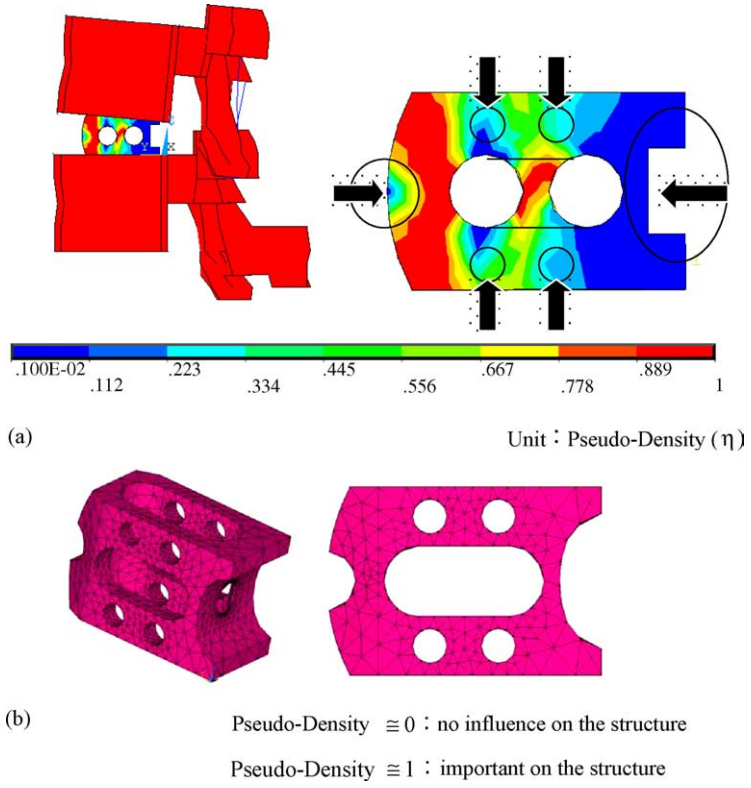

Fig. 3. Topology optimization analysis in flexion and the final design. (a) RF cage in the L2–L3 motion segment; the arrow and circle indicate the material shared less load and be removed and (b) FEM of the new design.

LS-RF and of the LS-NEW model were under 1.5° and were reduced by between 58% and 82%, respectively, in all motions when compared to the INT model. In lateral bending, the ROM of the LS-RF and of the LS-NEW fusion model were reduced by 81.15% and 81.54%, respectively, compared with the INT model. In flexion, these two fusion models had almost the same ROM (Fig. 4). Compared with a previous study, the trend of FEM calculation was similar to the trend of Morlock et al.'s [27] in vitro test in flexion, extension, and lateral bending as listed in Table 3.

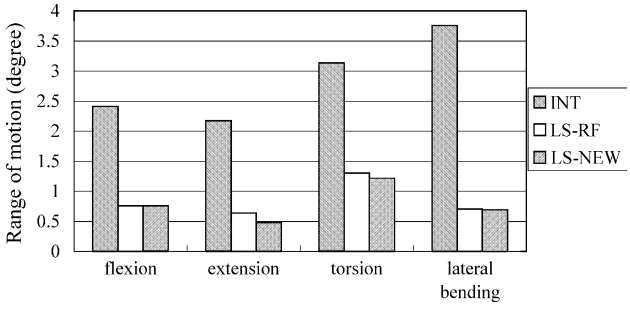

Fig. 4. Comparison of the ROM among the three FEMs.

3.2.2. *The maximum subsidence and dislodgement*

Subsidence of these two fusion models was relatively small as listed in Table 4; the LS-RF and LS-NEW models showed the greatest subsidence of about 0.089 mm and 0.087 mm in flexion, respectively. Dislodgement of the cage in the LS-NEW model occurred in torsion and was approximately 0.215 mm, with is slightly larger than that of the LS-RF model. Except for torsion, the value of dislodgement in the two FEMs was less than 0.03 mm.

3.2.3. *Stress of the adjacent disc*

In the LS-RF model, the maximum stress on the adjacent disc occurred in lateral bending with a magnitude of 1.27 MPa (Fig. 5). In flexion and extension, the disc stress of the two fusion models appeared to increase when compared with the

Table 3
Comparison of ROM decrease between the FEM calculation and the in vitro experiment

	Levels	Flexion (%)	Extension (%)	Torsion (%)	Lateral bending (%)
LS-RF model	L1–L3	69	71	58	81
LS-NEW model	L1–L3	67	78	61	82
Morlock et al. [25], with 10 N m, 150 N preload	L3–L5	86	89	34	75

Table 4
Comparison among all of the FEMs in the maximum subsidence, the maximum dislodgement, the maximum cage stress, and the maximum fixator stress

	Model	
	LS-RF	LS-NEW
Flexion		
Maximum subsidence (mm)	0.089	0.087
Maximum dislodgement (mm)	0.025	0.025
Maximum cage stress (MPa)	10.7	23.1
Maximum fixator stress (MPa)	73.4	73.5
Extension		
Maximum subsidence (mm)	0.008	0.008
Maximum dislodgement (mm)	0.008	0
Maximum cage stress (MPa)	0.3	0
Maximum fixator stress (MPa)	61.0	61.1
Torsion		
Maximum subsidence (mm)	0.037	0.036
Maximum dislodgement (mm)	0.171	0.215
Maximum cage stress (MPa)	26.3	47.7
Maximum fixator stress (MPa)	96.1	100.0
Lateral bending		
Maximum subsidence (mm)	0.052	0.048
Maximum dislodgement (mm)	0.016	0.029
Maximum cage stress (MPa)	44.9	43.2
Maximum fixator stress (MPa)	77.3	77.1

INT model, and the greatest rise reached 80%. The location of the maximum stress in the LS-RF and the LS-NEW model occurred in the anterior edge of the adjacent disc as shown in Fig. 6.

3.2.4. *Stress of the spinal cage*

In torsion, the maximum stress of the cage reached 47.7 MPa in the LS-NEW model. In lateral bending, the difference in the stress of the cage between these two fusion models was small. The stress of the cage in the LS-NEW model in flexion and torsion, respectively, increased by 116% and 81% when compared to that in the LS-RF model. As to stress distribution in flexion, the stress contour of the new cage was distributed more uniform than that of the RF cage, but the new cage generated higher stress than the RF cage as shown in Fig. 7.

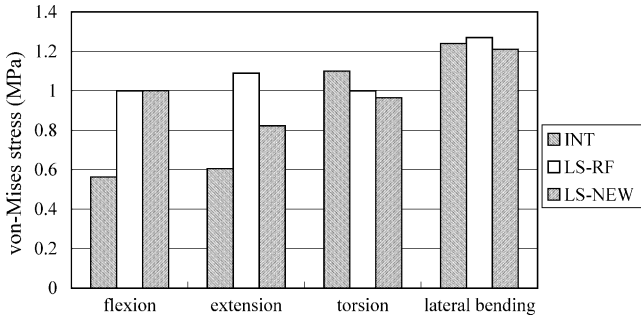

Fig. 5. The von-Mises stress of the adjacent disc.

4. Discussion

Posterior lumbar interbody fusion with a spinal cage aims to restore spinal stability, so many different kinds of cages have been developed in recent years. To evaluate biomechanical behavior of the present cage and design a new cage, this study conducted a finite element method to analyze stress distribution of lumbar spine with the cage. The results of this study confirmed that the present RF cage implant in the lumbar spine is able to achieve spinal stability. Furthermore, based on FEM calculations the performance of the new design cage was similar to that of the RF cage. However, compared to the in vitro test [27], some differences existed in our FEM, especially in torsion mode. The reason for this may be that the curvature of the FEM facet joint surface was not the same as curvature of the surface of the cadaveric specimen's facet joint, and linear simulation of the facet capsule in FEM might not represent an actual facet capsule.

Subsidence is a complication whereby the patient's disc height decreases, causing discomfort. Eck et al. [7] indicated that 14% of patients incurred the complication within a 2-year follow-up. The FEM results revealed that cage subsidence was likely to occur in flexion since the fused lumbar spine had the greatest ROM during this mode. This could easily cause the cage to sink into the cancellous bone because of higher contact stresses. Linde [28] reported a failure stress of 4 MPa for cancellous bone. Therefore, this value was taken to be the failure stress of a vertebral body. Compared with Linde's study, our maximum von-Mises stress in cancellous bone was still lower than the failure stress. Therefore, we believed that the cage subsidence was within the elastic region. In addition, Carl et al. [8] reported the complication of dislodgement that occurred in approximately 1.4% of cases. However, it is unclear what the biomechanical mechanism is that causes this complication. Kim [12] indicated that the maximum dislodgement occurs in torsion with a preload, which is consistent with our FEM calculation. However, our FEM also found that subsidence and dislodgement of the cage was unlikely to happen simultaneously. From a mechanical viewpoint, the stability of the cage was increased as a result of contact stress between the cage and the vertebral body. Therefore, one can logically conclude that the cage in flexion can possibly induce more contact stress and cause subsidence, but this lowers the opportunity of dislodgement.

Zou et al. [29] addressed that the cage with its large central opening and more bone chips generates more new bone formation in the hole. Based on the research, we believe that topology optimized design of new cage would reduce the volume of cage to place more bone graft and facilitate bony fusion without affecting the spinal stability. In topology optimization, the study reduced the volume of the RF cage by approximately 36% to form the new cage. This new cage can afford similarly sufficient stability to the lumbar spine with laminectomy as the RF cage can. Moreover, the stress distribution of the LS-NEW model was similar to that of the LS-RF model as shown in Fig. 6. The advantage of the more porous

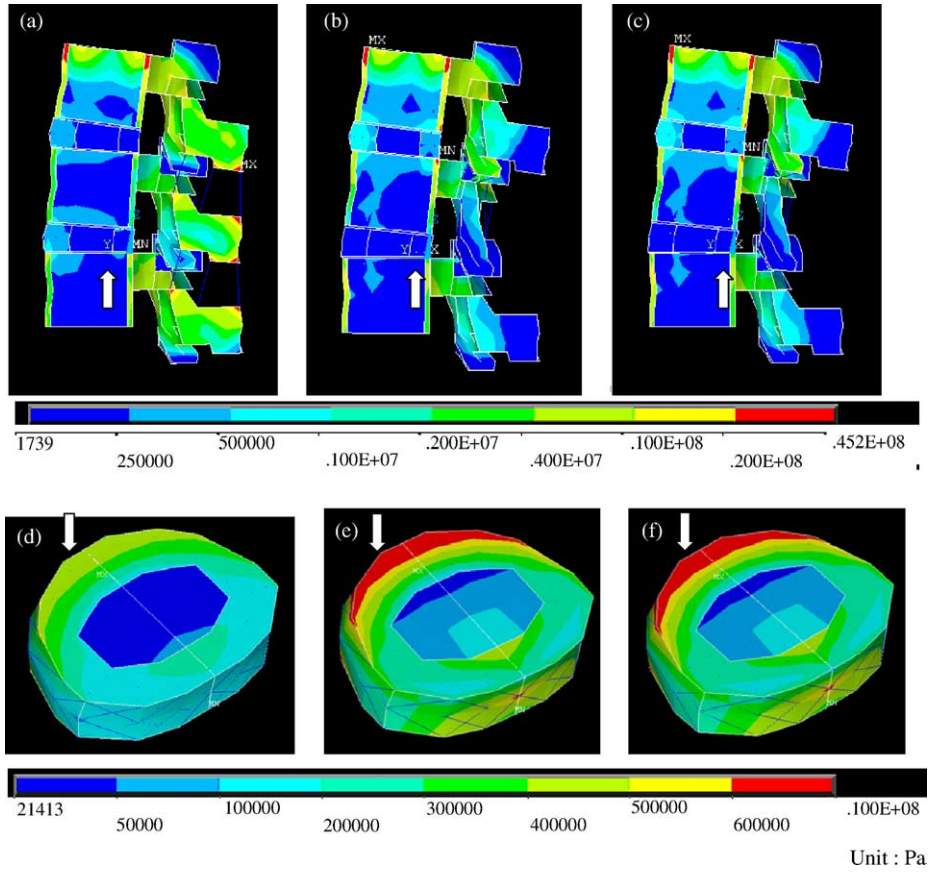

Fig. 6. The von-Mises stress distribution of the lumbar spine L1–L3 and the adjacent disc L1–L2 in flexion. (a) INT model, (b) LS-RF model, (c) LS-NEW model, (d) adjacent disc L1–L2 in the INT model, (e) adjacent disc L1–L2 in the LS-RF model, and (f) adjacent disc L1–L2 in the LS-NEW model. The arrow indicates the stress change of disc L2–L3 among the three FEMs. After implanting spinal cage, the stress of the adjacent disc L1–L2 remarkably increased and concentrated on anterior edge.

new cage is that it allows more bone graft for enhanced bony fusion to be placed, but the disadvantage is that the new cage raised more stress than the RF cage. Although stress in the new cage increased remarkably, the stress of the cage was still much lower than the yield strength of the titanium alloy (848.4 MPa) [30]. Additionally, the cage is usually combined with a spinal fixator for stabilizing the lumbar spine. In clinical observations [2,7], fixator failure occurs more frequently than cage failure. In our FE analysis, the fixator stress was greater than the cage stress under the same material usage as listed in Table 4, so the risk of spinal fixator failure occurred more frequently than cage breakage.

Kuslich et al. [9] reported in a 4-year follow-up study on cage implants that early degeneration of the adjacent disc had been reported in 5.6% of his patients. Compared with the INT model, the adjacent disc stress with the LS-RF and the LS-NEW models would rise substantially in flexion, but this research simulated nonunion in the postoperative early

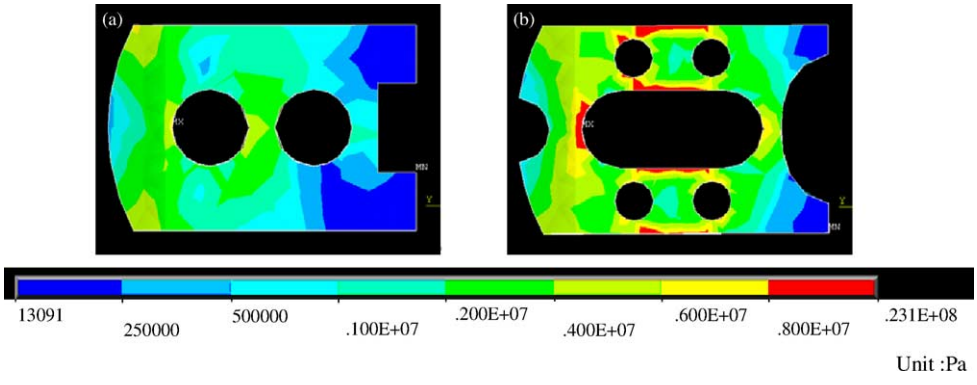

Fig. 7. Comparison of the von-Mises stress between the RF and the new cage in flexion. (a) RF cage and (b) new cage.

stage and the bone graft was not fused to the vertebral body. Consequently, the stress on the adjacent disc could possibly increase further since the bone graft completely fusing to the vertebral body would give rise to greater stiffness of the motion segment. As a result, accelerated degeneration of the adjacent disc is possible under a situation of stress concentration as shown by clinical observation. The adjacent disc stress contour also produced the same results between the spine with the new cage and with the existing cage as shown in Fig. 6. The reason was because the new and existing cages had almost the same biomechanical influence on the entire spine and adjacent disc.

Regarding the limitation and restriction of this study, the material properties used in this FEM, namely nonlinear behavior of spinal ligaments, viscoelasticity of the disc, degeneration of the disc, and orthotropic characteristics of the vertebral body [21–23], were different from those of the cadaver specimen. Our study did not simulate disc degeneration because of the broad definition of disc degeneration, such as delamination or dehydration. No study has addressed the correct material parameters of a degenerated disc. What we could do was to apply the correct spinal surgery procedure to analyze the biomechanical influence on cage shape. The effect of these FEM simulations was similar to that of the in vitro test. Therefore, muscle contraction, complicated external load, movement of the pelvis, and completeness of the entire spine were not considered in this study. In the clinic, when spinal cages are implanted, the disc space is distracted, leading to tension in the annular fibers. It is believed that the contracting fibers produce compression between the cage and the vertebrae, maintaining the cage in place. The mechanism is called the distraction-compression principle [1]. In our study, this mechanism was not modeled.

5. Conclusions

The new cage was shaped by topology optimization and decreased the volume of the present RF cage by approximately 36%, but this new design was still able to afford as much spinal stability as the RF cage. Additionally, the biomechanical parameters of the new design cage produced almost the same performance, in terms of subsidence, stress of adjacent disc and ROM, as the RF cage. The advantage of the new cage is that it increased the space to place bone graft, reduced the material cost of the cage and generated less subsidence than the existing cage under the four different loading conditions. The disadvantage is that it increased the machining expense for manufacture, and the cage generated higher stresses, but these were still much lower than the yield strength of the cage material.

Acknowledgement

The research was made possible through grants from Department of Health (DOH92-TD-1118), Taiwan.

References

[1] Bagby GW. Arthrodesis by the distraction–compression method using a stainless steel implant. Orthopedics 1988;11:931–4.
[2] McAfee PC. Interbody fusion cages in reconstructive operations on the spine. J Bone Joint Surg [Am] 1999;81-A(6):859–80.
[3] Matge G. Cervical cages fusion with 5 different implants: 250 cases. Acta Neurochir 2002;144(6):539–49.
[4] Brantigan JW, McAfee PC, Cunningham BW, Wang H, Orbegoso CM. Interbody lumbar fusion using a carbon fiber cage implant versus allograft bone. An investigational study in the Spanish goat. Spine 1994;19(13):1436–44.
[5] Ray CD. Threaded titanium cages for lumbar interbody fusions. Spine 1997;22(6):667–79.
[6] Brantigan JW, Steffee AD. A carbon fiber implant to aid interbody lumbar fusion: two-year clinical results in the first 26 patients. Spine 1993;18(14):2106–17.
[7] Eck KR, Bridwell KH, Ungacta FF, Lapp MA, Lenke LG, Riew KD. Analysis of titanium mesh cages in adults with minimum two-year follow-up. Spine 2000;25(18):2407–15.
[8] Carl AL, Kostuick JP, Abitbol JJ, et al. Interdiscal cage complications: a general consensus. In: Annual Meeting of the North American Spine Society. 1999.
[9] Kuslich SD, Danielson G, Dowdle JD, Sherman J, Fredrickson B, Yuan H, et al. Four-year follow-up results of lumbar spine arthrodesis using the Bagby and Kuslich lumbar fusion cages. Spine 2000;25(20):2656–62.
[10] Pitzen T, Geisler FH, Matthis D, Muller-Storz H, Steudel WI. Motion of threaded cages in posterior lumbar interbody fusion. Eur Spine J 2000;9:571–6.
[11] Pitzen T, Geisler FH, Matthis D, Muller-Storz H, Pedersen K, Steudel WI. The influence of cancellous bone density on load shearing in human lumbar spine: a compression between an intact and surgically altered motion segment. Eur Spine J 2001;10:23–9.
[12] Kim Y. Prediction of mechanical behaviors at interfaces between bone and two interbody cages of lumbar spine segments. Spine 2001;26(13):1437–42.
[13] Pitzen T, Matthis D, Steudel WI. The effect of posterior instrumentation following PLIF with BAK cages is most pronounced in weak bone. Acta Neurochir (Wien) 2002;144(2):121–8.
[14] Palm WJ, Rosenberg WS, Keaveny TM. Load transfer mechanisms in cylindrical interdody cages constructs. Spine 2002;27(19):2101–7.
[15] Polikeit A, Ferguson SJ, Nolte LP, Orr TE. Factors influencing stresses in the lumbar spine after the insertion of intervertebral cages: finite element analysis. Eur Spine J 2002;12(4):413–20.
[16] Adam C, Pearcy M, McCombe P. Stress analysis of interbody fusion—finite element modeling of intervertebral implant and vertebral body. Clin Biomech 2003;18:265–72.
[17] Goel VK, Monroe BT, Gilbertson LG, Brinckmann P. Interlaminar shear stresses and laminae separation in a disc. Finite element analysis of the L3–L4 motion segment subjected to axial compressive loads. Spine 1995;20(6):689–98.
[18] Wu HC, Yao RF. Mechanical behavior of the human annulus fibrosus. J Biomech 1967;(9):1–7.
[19] Yamada H. In: Evans FG, editor. Strength of biological materials. Baltimore: Williams & Wilkins; 1970. p. 73–8.
[20] Agur AMR, Lee MJ. Grant's atlas of anatomy. 10th ed. Williams & Wilkins Lippincott; 1999.
[21] Chen CS, Cheng CK, Liu CL, Lo WH. Stress analysis of the disc adjacent fusion in lumbar spine. Med Eng Phys 2001;23:483–91.
[22] Chen CS, Cheng CK, Liu CL. A biomechanical comparison of posterolateral fusion and posterior fusion in the lumbar spine. J Spinal Disord Tech 2002;15(1):53–63.
[23] Chen CS, Feng CK, Cheng CK, Tzeng MJ, Liu CL, Chen WJ. Biomechanical analysis of the disc adjacent to posterolateral fusion with laminectomy in lumbar spine. J Spinal Disorder Tech 2005;18(1):58–65.

[24] Svehla M, McCoombe P, Stanford R, Walsh W. Can autograft stiffen interbody fusion cages? 47th Annual Meeting. 2001.
[25] ANSYS Inc. Theory Reference Release 6.0.
[26] Yamamoto I, Panjabi MM, Crisco T, Oxland T. Three-dimension movement of the whole lumbar spine and lumbosacral joint. Spine 1989;14(11):1256–60.
[27] Morlock MM, Strandborg J, Nassutt R, Sellenschloh K, Eggers C. Primary stability of dorsal lumbar spondylodesis and vertebral body replacement surgery—comparison of different vertebral body replacement cages in-vitro. In: 47th Annual Meeting. 2001.
[28] Linde F. Elastic and viscoelastic properties of trabecular bone by a compression testing approach. Dan Med Bull 1994;41:119–38.
[29] Zou X, Li H, Bunger M, Egund N, Lind M, Bunger C. Bone ingrowth characteristics of porous tantalum and carbon fiber interbody device: an experimental study in pigs. Spine J 2004;4:99–105.
[30] Wood RA, Favor BJ. Titanium Alloy Handbook. Airforce Materials Laboratory. Metals, Ceramics Information Center, 1972.